Mechanical Characterization of Lead-Free Sn-Ag-Cu Solder Joints by High-Temperature Nanoindentation

S. LOTFIAN,[1] J.M. MOLINA-ALDAREGUIA,[1,4] K.E. YAZZIE,[3]
J. LLORCA,[1,2] and N. CHAWLA[3]

The reliability of Pb-free solder joints is controlled by their microstructural constituents. Therefore, knowledge of the solder microconstituents' mechanical properties as a function of temperature is required. Sn-Ag-Cu lead-free solder alloy contains three phases: a Sn-rich phase, and the intermetallic compounds (IMCs) Cu_6Sn_5 and Ag_3Sn. Typically, the Sn-rich phase is surrounded by a eutectic mixture of β-Sn, Cu_6Sn_5, and Ag_3Sn. In this paper, we report on the Young's modulus and hardness of the Cu_6Sn_5 and Cu_3Sn IMCs, the β-Sn phase, and the eutectic compound, as measured by nanoindentation at elevated temperatures. For both the β-Sn phase and the eutectic compound, the hardness and Young's modulus exhibited strong temperature dependence. In the case of the intermetallics, this temperature dependence is observed for Cu_6Sn_5, but the mechanical properties of Cu_3Sn are more stable up to 200°C.

INTRODUCTION

The elimination of lead from electronics due to its detrimental effects on the environment and health is pushing component manufacturers to use Pb-free alloys.[1–8] Replacing Sn-Pb with Pb-free solders has resulted in widespread study of materials properties, processing technology, and reliability.[9,10] During service, interconnects will be exposed to relatively high temperatures, and the thermomechanical reliability of solder joints will be greatly affected by the mechanical properties of the individual microconstituents in the solder alloy; For instance, in the case of Sn-Ag-Cu (SAC) lead-free solder alloys, the solder contains three phases: a Sn-rich β-Sn phase, and the intermetallic compounds (IMCs) Cu_6Sn_5 and Ag_3Sn. The microstructure consists of Sn-rich dendrites surrounded by a eutectic mixture of β-Sn and Ag_3Sn, with small amounts of Cu_6Sn_5. Reflow of the solder material on Cu typically results in formation of Cu-Sn intermetallic layers at the solder–Cu interface, which can influence the properties of the solder joint. Therefore, new methods are required to assess the mechanical properties of these phases, not only at room temperature but also at the high temperatures encountered in service.[9,11]

Previous studies have mainly focused on the room-temperature mechanical response of the individual phases.[1,2,9,12–14] In this paper we report on high-temperature nanoindentation measurements of Young's modulus and hardness of several microconstituents in a Sn-3.9Ag-0.7Cu solder, in order to study the temperature dependence of the individual phases. Knowledge of the mechanical properties of individual phases as a function of temperature will be invaluable for obtaining a better understanding of the temperature-dependent behavior of these materials. It will also be invaluable in developing accurate constitutive equations for modeling solder joint behavior.

EXPERIMENTAL PROCEDURES

Sn-3.9Ag-0.7Cu solder joints were prepared by melting Sn-3.9Ag-0.7Cu pellets (Indium Corp., Utica, NY, USA) between two polished oxygen-free high-conductivity Cu bars on a digital programmable hot plate (Torrey Pines Scientific, San Marcos, CA, USA). Details of the reflow procedure can be obtained elsewhere.[15] The processing conditions were controlled in order to obtain two types of joints: (a) one with a thinner intermetallic layer but coarser solder microstructure, and (b) one with a relatively thick intermetallic layer but finer solder microstructures, as shown in Fig. 1. Joints of type (a) were used to obtain the properties of the pure β-Sn phase. The size of the intermetallic layer formed at the solder–Cu interface in type (a) joints was not sufficiently thick to provide accurate results from indentation. However, joints of type (b) enabled characterization of the Cu-Sn intermetallic layers and the eutectic compound. Both types of joints were heated to 20°C above the melting point of Sn-3.9Ag-0.7Cu, but were reflowed for different times: 40 s for joints of type (a) and 168 h for type (b). All samples were cut, and polished to a 0.05-μm finish, with colloidal silica.

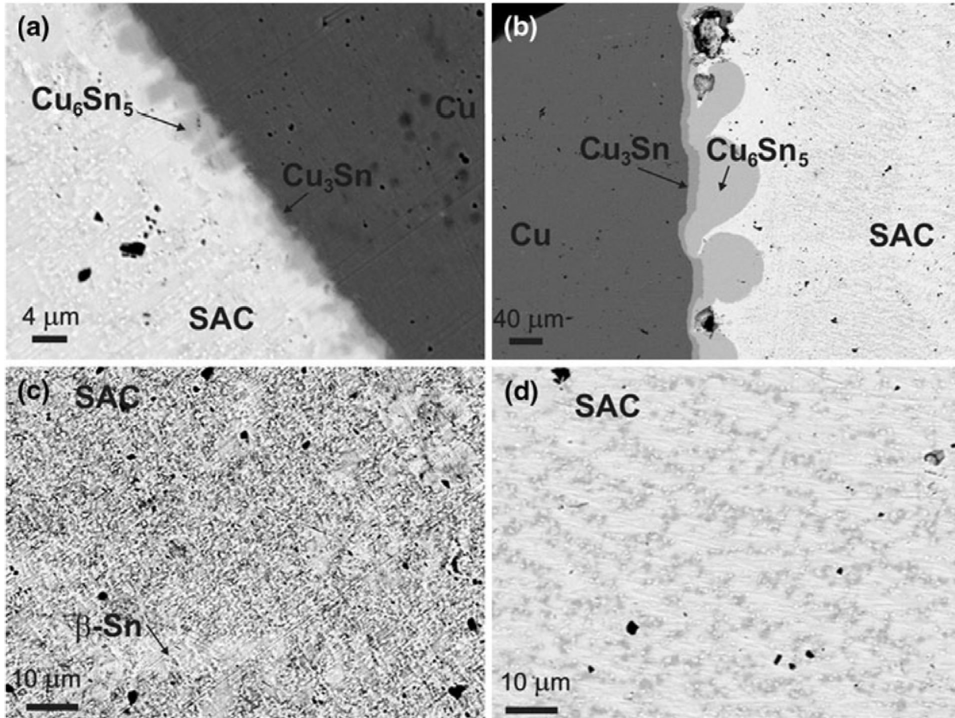

Fig. 1. Scanning electron microscopy (SEM) image of the Cu–SAC interface for (a) 40 s and (b) 168 h reflow time at 240°C. Detail of the microstructure of the SAC for (c) 40 s and (d) 168 h reflow time.

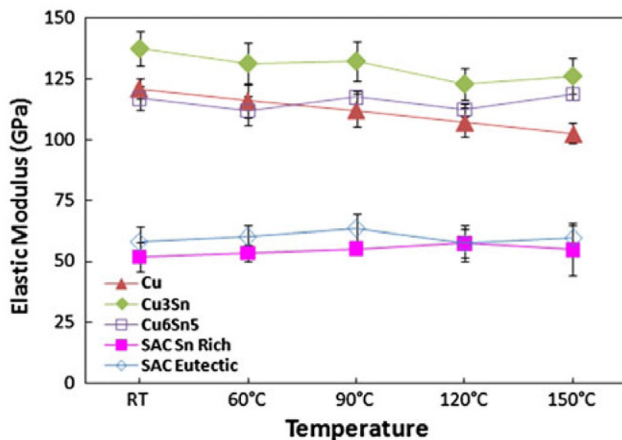

Fig. 2. Elastic modulus of each microconstituent as a function of temperature.

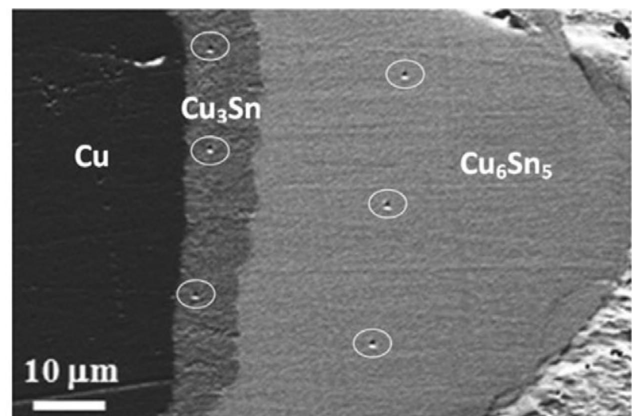

Fig. 3. Interface microstructure of SAC joint, showing Cu_6Sn_5 and Cu_3Sn intermetallics.

Table I. Elastic modulus of the different phases in the SAC solder joint

Elastic Modulus (GPa)	RT	60°C	90°C	120°C	150°C
Cu	121 ± 4	116 ± 6	112 ± 6	107 ± 6	103 ± 4
Cu_3Sn	138 ± 7	132 ± 8	132 ± 8	123 ± 6	126 ± 7
Cu_6Sn_5	117 ± 5	111 ± 6	117 ± 2	112 ± 2	118 ± 2
Eutectic phase	57 ± 6	60 ± 5	63 ± 6	57 ± 7	60 ± 5
Sn-rich phase	52 ± 6	53 ± 3	55 ± 2	57 ± 5	55 ± 10

Table II. Hardness of the different phases in the SAC solder joint

Hardness (GPa)	RT	60°C	90°C	120°C	150°C
Cu	1.8 ± 0.1	1.7 ± 0.2	1.6 ± 0.1	1.54 ± 0.06	1.4 ± 0.1
Cu_3Sn	6.7 ± 0.5	6.4 ± 0.5	6.4 ± 0.6	5.6 ± 0.4	5.2 ± 0.6
Cu_6Sn_5	6.7 ± 0.4	6.6 ± 0.6	6.4 ± 0.2	5.1 ± 0.1	3.9 ± 0.3
Eutectic phase	0.58 ± 0.01	0.37 ± 0.05	0.31 ± 0.05	0.22 ± 0.03	0.16 ± 0.02
Sn-rich phase	0.31 ± 0.01	0.28 ± 0.01	0.26 ± 0.01	0.19 ± 0.01	0.15 ± 0.01

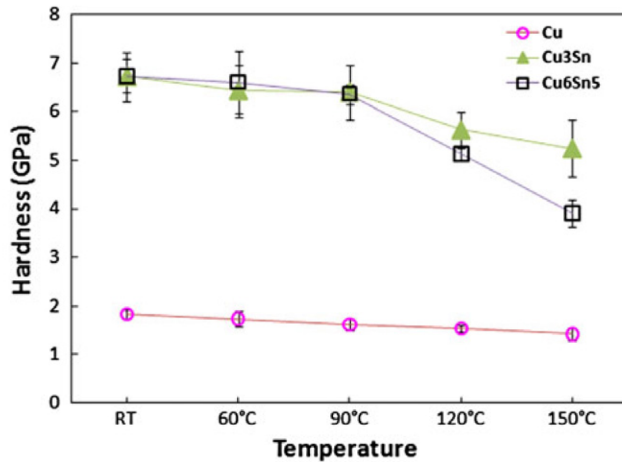

Fig. 4. Hardness of copper, Cu_3Sn, and Cu_6Sn_5.

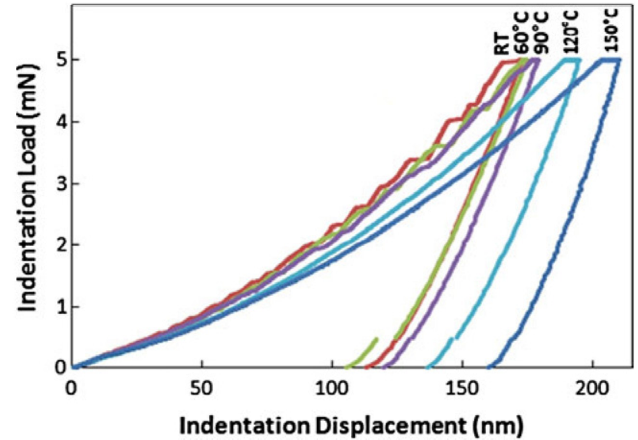

Fig. 5. Indentation load–displacement curves of Cu_6Sn_5 at different temperatures.

Nanoindentation testing was carried out using a TI 950 Triboindenter™ (Hysitron, Inc., Minneapolis, MN). The indentation tip assembly consists of a Berkovich-geometry diamond tip brazed to a low thermal expansion coefficient Zerodur® shaft, attached directly to the load transducer behind a heat shield. Nanoindentation testing was carried out at room temperature, 60°C, 90°C, 120°C, and 150°C. Ten different samples were used, one for each test temperature. Each sample was placed on the heater plate and subsequently heated to the target temperature. The indenter was then placed in contact with the sample using a small contact load (2 μN), and contact was maintained for at least 30 min prior to the first indentation test, to allow for thermal stabilization of the system. Using this approach, typical drift rates of 0.1 nm s^{-1} were achieved. Two types of indentation tests were carried out at room temperature: conventional loading–unloading up to a maximum load of 5 mN, and multiple loading–unloading cycles to extract hardness and modulus as a function of indentation depth. The indentations were carried out at a loading rate of 2.5 mN s^{-1} with a hold period of 0.2 s at maximum load. This procedure helped to minimize creep effects on the measurement of the Young's modulus from the unloading stiffness. Upon unloading, drift was measured by introducing a 20 s hold segment at 10% of the maximum load. The drift rate was measured over the last 10 s of the hold segment. At least 10 indentations were performed at each temperature, and the samples were kept at the test temperature for at least 4 h. The load

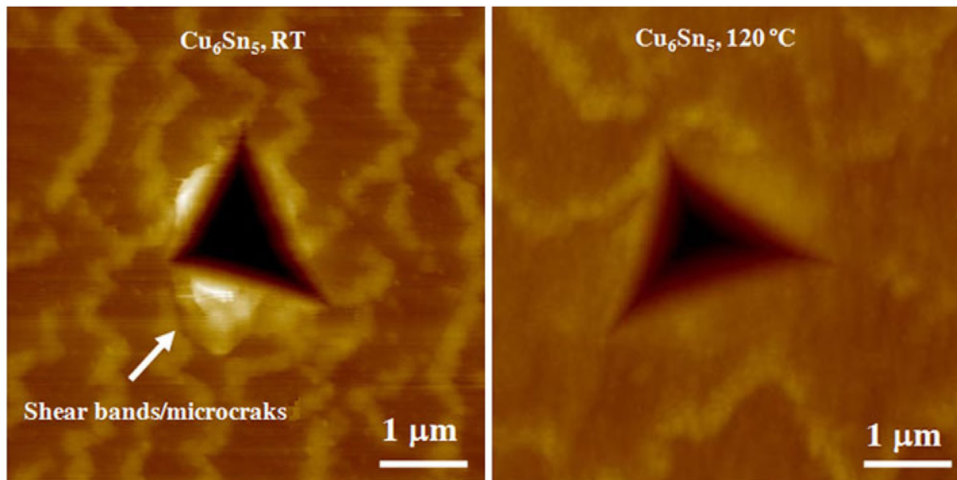

Fig. 6. AFM surface morphology of indentation in Cu_6Sn_5 at RT and 120°C.

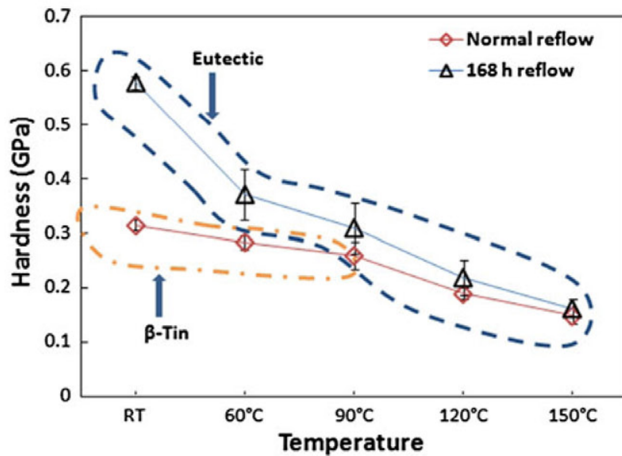

Fig. 7. Hardness of phases in SAC solder: Sn-rich phase and eutectic.

–displacement curves were analyzed using the Oliver and Pharr method.[16]

To carry out a more detailed analysis, selected indentations were further characterized by atomic force microscopy (AFM) to study pile-up/sink-in effects using a Park XE-150 instrument (Park Systems, Suwon, Korea). Scanning electron microscopy (SEM, EVO® MA15; Carl Zeiss) provided microstructural details, such us the distribution of phases in the solder and the intermetallic interlayer thicknesses. Chemical analysis was performed by energy-dispersive spectroscopy (EDS) using an Oxford INCA 350 microanalysis system attached to the SEM.

RESULTS AND DISCUSSION

Figure 2 plots the elastic modulus of each phase in the solder joint with increasing temperature, assuming the following Poisson's ratios for each phase: 0.3 for Cu_3Sn, 0.31 for Cu_6Sn_5, 0.34 for copper, and 0.4 for the SAC solder (close to the Poisson's ratio for pure Sn)[14]. Results for the indentation modulus at room temperature are in good agreement with published studies on bulk alloys or solder joints.[1,2] Figure 2 shows that the Young's moduli of the two intermetallics remain almost constant with temperature, while the elastic modulus of copper decreases around 15% at 150°C, in good agreement with literature data for Cu.[17] In the case of the SAC solder, due to the size of the β-Sn grains and the β-Sn/Ag_3Sn eutectic domains, only small 2-mN indents were performed to ensure that the indents were fully contained in a single phase/domain. In both cases, the elastic moduli were relatively insensitive to temperature, with an average elastic modulus at room temperature of 52 GPa for the Sn-rich phase and 68 GPa for the eutectic. This can be explained by the higher modulus (~90 GPa) of the Ag_3Sn particles embedded in the Sn matrix. The elastic modulus results are summarized in Table I, where the errors represent one standard deviation.

Figure 3 shows the microstructure of the sample reflowed for 168 h. Large intermetallic layers of Cu_6Sn_5 and Cu_3Sn were observed. Note that the indentations are much smaller than the intermetallic phase thickness, and reside completely within a layer. Figures 1 and 3 show that the initial morphology of the intermetallic interlayers was very much dependent upon thermal aging. The Cu_3Sn layer had a planar morphology and consisted of finer, columnar grain structure, compared with Cu_6Sn_5 that formed as large scallops due to a thermal grooving mechanism, as discussed in previous studies.[2,15,18,19]

The hardness results are summarized in Table II. Figure 4 shows the hardness of the copper substrate and the two IMCs. The decrease in the hardness of

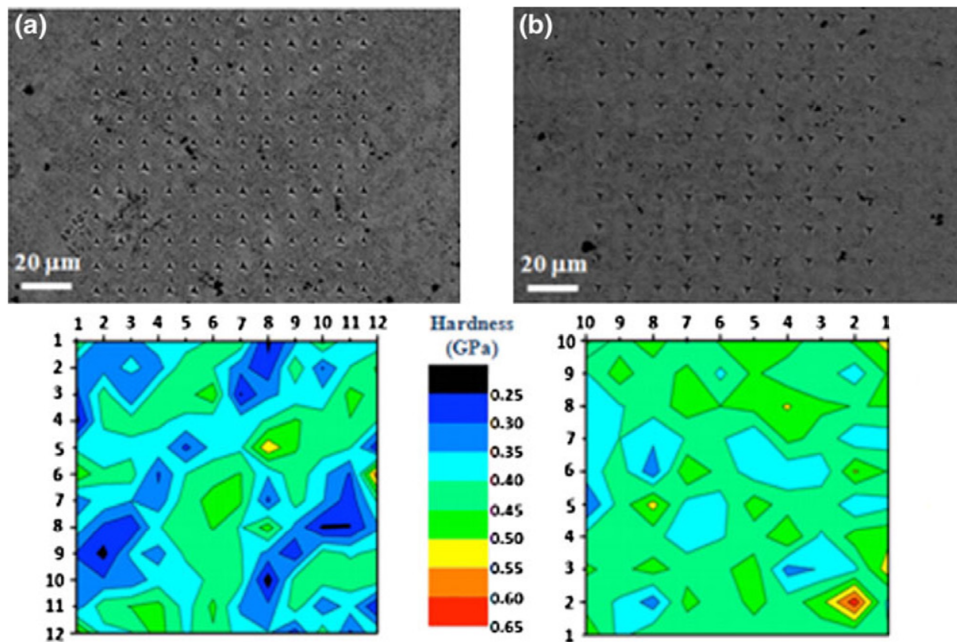

Fig. 8. Hardness map at room temperature of reflowed samples: (a) 40 s reflow time and (b) 168 h reflow time.

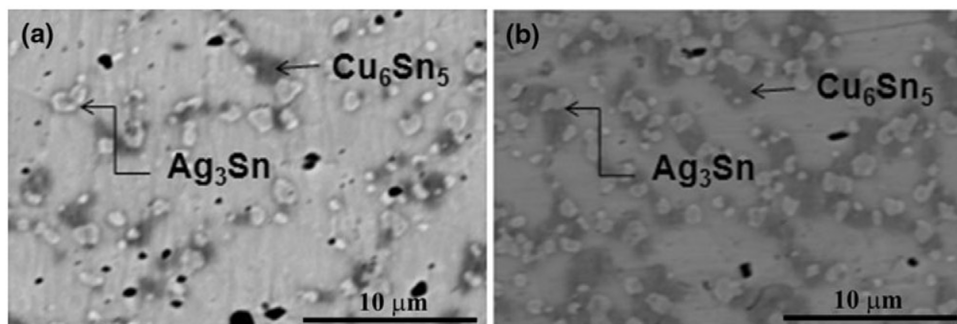

Fig. 9. Evolution of the microstructure during high-temperature (150°C) testing of the samples for (a) 40 s reflow time and (b) 168 h reflow time.

Cu is consistent with the expected behavior for pure Cu. The two intermetallics show a distinct behavior, with constant hardness up to 90°C, after which the hardness starts to decrease, more strongly in the case of Cu_6Sn_5. The drop in hardness in Cu_6Sn_5, and to a lesser extent in Cu_3Sn, is accompanied by a change in the appearance of the load–displacement curves before and after 90°C, as shown in Fig. 5.

The load–displacement curves below 90°C show multiple pop-ins, characteristic of shear band formation or microcracking.[20] Above 90°C, the curves are smooth, with no evidence of cracking, and characteristic of a more ductile deformation behavior. The results suggest a brittle-to-ductile transition in the deformation behavior of the intermetallic phases (Fig. 5). AFM was used to quantify the surface profile of the indentations in each phase. The topography results in Cu_6Sn_5 show distinct features in the deformation pattern below and above 90°C. At room temperature, the pile-up around the indent contrasts with a more homogeneous flow around the indentations at 120°C. The pile-up at room temperature shows abrupt steps, but does not give rise to an increase in the contact area. This is indicative of the formation of shear bands and/or microcracks, which can explain the multiple pop-ins observed during loading below 90°C (Fig. 6). These features are not observed at 120°C, which, together with the smoother loading behavior, reinforces the suggested brittle-to-ductile transition in the behavior of both Cu_3Sn and Cu_6Sn_5 intermetallics. This brittle-to-ductile transition might be associated with the activation of dislocation flow, which explains the stronger temperature dependence observed in the hardness at temperatures above 90°C in Fig. 3. However, careful transmission electron microscopy (TEM) study of the area under the indents would be required to confirm this.

In the case of the SAC solder, the difference in hardness between the β-Sn-rich phase and the eutectic compound is $\sim$100% at room temperature, but this difference tends to decrease with temperature, with the

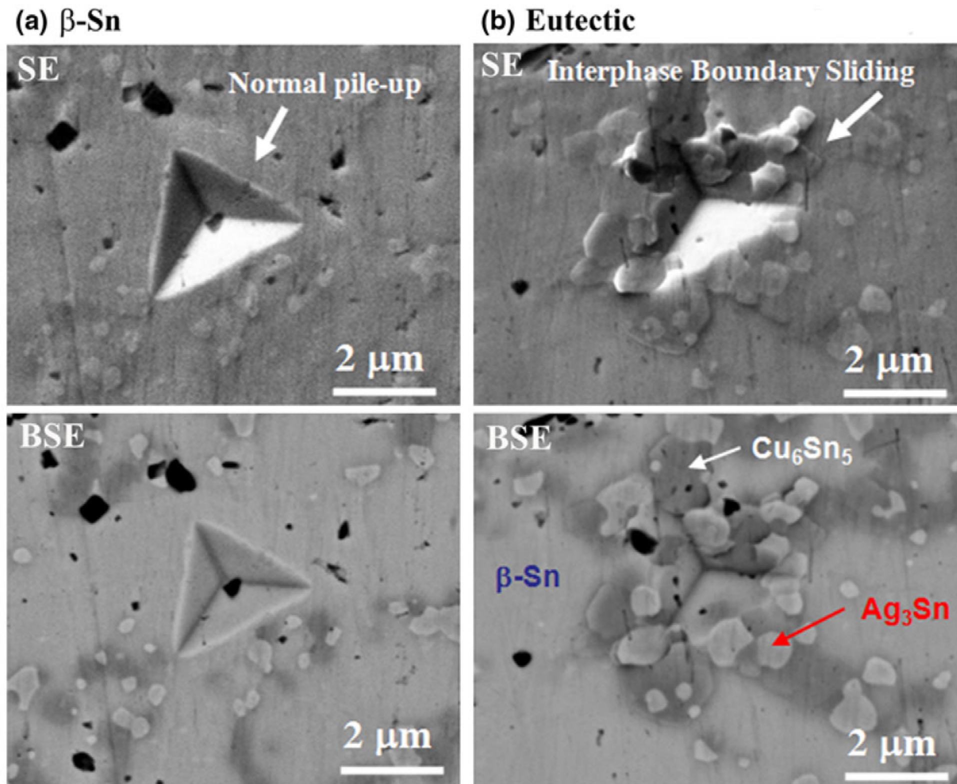

Fig. 10. Secondary electron (SE) and backscatter electron (BSE) images of indentation imprints on (a) β-Sn and (b) the eutectic compound.

hardness being identical at 150°C (Fig. 7; Table II). The reported Ag_3Sn hardness at room temperature is 3.2 GPa, measured in bulk samples, which is consistent with the hardness difference between the β-Sn-rich phase and the eutectic compound[1] at room temperature.

However, the evolution with temperature is more difficult to understand. The results suggest that above 90°C both β-Sn and the eutectic compound display the same hardness, but we believe that this is due to the microstructural evolution of the solder material at the high temperature of the tests (homologous temperatures higher than 0.7). Indeed, Fig. 8 plots hardness maps for the two initial samples studied: (a) normal reflow and (b) 168 h reflow. The maps correlate well with the initial microstructure and the distribution of Ag_3Sn and Cu_6Sn_5 particles within the β-Sn phase (Fig. 8).

In this sense, sample (a) initially contained larger β-Sn-rich particles where the hardness of this phase could be computed at room temperature, while the solder in sample (b) presented a more homogeneous microstructure, so that the hardness is representative of the eutectic compound. However, it was noticed that, for testing temperatures above 90°C, the microstructure in sample (a) tended to homogenize, so that the microstructures of both samples were identical at testing temperatures of 150°C (Fig. 9). Therefore, the results in Fig. 7 corresponding to the sample with the 40 s reflow time can only be attributed to β-Sn up to 90°C, while for higher temperatures both samples provided the same results, corresponding to the eutectic compound.

According to these results, it is clear from Fig. 7 that the temperature dependence of the hardness is much stronger for the eutectic compound than for the β-Sn phase. This is expected based on the major contribution of interface sliding and coarsening of Ag_3Sn in the case of the eutectic compound, as demonstrated in Fig. 10. Figure 10a shows a residual imprint in β-Sn phase showing a homogeneous deformation pattern. However, Fig. 10b shows the corresponding residual imprint in the eutectic, showing the major contribution of interphase boundary sliding in this case (Fig. 9), which can explain the strong temperature dependence of the hardness results.

CONCLUSIONS

High-temperature nanoindentation has proven very useful to measure the Young's modulus and hardness values of the individual phases present in a Sn-3.9Ag-0.7Cu solder joint as a function of temperature. In particular, the properties of the Cu_6Sn_5 and Cu_3Sn intermetallics, the β-Sn phase, and the SAC eutectic compound have been measured in the temperature range between room temperature and 150°C. The results at room temperature are in good

agreement with previous results. No data have been reported so far at high temperatures, but our results suggest that the Cu_6Sn_5 and Cu_3Sn intermetallics display a brittle-to-ductile transition at 90°C. In the case of β-Sn, it is not possible to assess the properties of β-Sn dendrites at temperatures above 90°C, due to the homogenization of the microstructure at the testing temperature. The hardness of the eutectic Sn-3.9Ag-0.7Cu compound displays a very strong temperature dependence, presumably due to the role of interphase boundary sliding in the mechanical properties. Accurate and reliable determination of the hardness and Young's modulus values of these phases is of great importance for the study of the mechanical reliability of solder joints.

ACKNOWLEDGEMENTS

S.L., J.M.M.-A., and J.L. acknowledge the financial support of the Spanish Ministry of Science and Innovation (MAT2009-14396) and the Comunidad de Madrid through the program ESTRUMAT (S2009/MAT-1585). K.E.Y. and N.C. are grateful for the financial support for this work from the United States National Science Foundation Division of Materials Research–Metals Division (Drs. Alan Ardell, Bruce MacDonald, and Harsh Chopra, Program Directors).

REFERENCES

1. X. Deng, N. Chawla, K.K. Chawla, and M. Koopman, *Acta Mater.* 52, 4291 (2004).
2. X. Deng, M. Koopman, N. Chawla, and K.K. Chawla, *Mater. Sci. Eng. A* 364, 240 (2004).
3. F. Gao and T. Takemoto, *Mater. Lett.* 60, 2315 (2006).
4. J. Glazer, *Int. Mater. Rev.* 40, 65 (1995).
5. J. Glazer, *J. Electron. Mater.* 23, 693 (1994).
6. M. McCormack and S. Jin, *JOM* 45(7), 36 (1993).
7. W.J. Plumbridge, *J. Mater. Sci.* 31, 2501 (1996).
8. P. Vianco and D. Frear, *JOM* 45(7), 14 (1993).
9. N. Chawla, *Int. Mater. Rev.* 54, 368 (2009).
10. H. Zhiheng, L. Changqing, P. Conway, and R. Thomson, *HDP '04. Proceeding of the Sixth IEEE CPMT Conference*, vol. 52 (2004).
11. F. Gao, H. Nishikawa, T. Takemoto, and J. Qu, *Microelectron. Reliab.* 49, 296 (2009).
12. R.R. Chromik, R.P. Vinci, S.L. Allen, and M.R. Notis, *J. Mater. Res.* 18, 2251 (2003).
13. Y. Sun, J. Liang, Z.-H. Xu, G. Wang, and X. Li, *J. Mater. Sci. Mater. Electron.* 19, 514 (2007).
14. P.-F. Yang, Y.-S. Lai, S.-R. Jian, J. Chen, and R.-S. Chen, *Mater. Sci. Eng. A* 485, 305 (2008).
15. X. Deng, G. Piotrowski, J.J. Williams, and N. Chawla, *J. Electron. Mater.* 32, 1403 (2003).
16. W.C. Oliver and G.M. Pharr, *J. Mater. Res.* 7, 1564 (1992).
17. J.C. Trenkle, C.E. Packard, and C.A. Schuh, *Rev. Sci. Instrum.* 81, 073901 (2010).
18. F. Guo, S. Choi, J.P. Lucas, and K.N. Subramanian, *J. Electron. Mater.* 29, 1241 (2000).
19. G. Zeng, S. Xue, L. Zhang, L. Gao, W. Dai, and J. Luo, *J. Mater. Sci. Mater. Electron.* 21, 421 (2010).
20. L. Jiang and N. Chawla, *Scripta Mater.* 63, 480 (2010).